Maíra M. Garcia*, Tiago R. Oliveira, Khallil T. Chaim, Maria C. G. Otaduy, Christian Bruns, Jan T. Svejda, Johannes Bernarding, Daniel Erni, and Waldemar Zylka

Thermal measurements of a muscle-mimicking phantom during ultra-high field magnetic resonance imaging

https://doi.org/10.1515/cdbme-2023-1080

Abstract: At ultra-high field MRI ($B_0 \geq 7$T) it is crucial to predict and control the patient safety. Commonly patient safety is controlled by the power deposited in the tissue (specific absorption rate - SAR). However, temperature distributions do not always correlate directly with SAR distributions, which makes temperature control also a crucial parameter to guarantee patient safety. In this work, temperature changes were accessed by MR thermometry, specifically by the proton resonance frequency shift technique (PRF). A phantom mimicking muscle tissue was used to evaluate the temperature rise caused by the radiofrequency (RF) absorption during 7T MRI, applied through a commercial birdcage head coil. A pulse-sequence protocol was implemented for both, the generation of temperature increase and the MR thermometry. To control the temperature, a digital thermometer was used, and oil tubes were utilized to dismiss the B_0 drift effects for PRF. Measurements of the phantom's dielectric characteristics, i.e. conductivity and permittivity, were in good agreement with the literature values for muscle. Spatio-temporal evaluations showed a temperature increase in time via RF exposure and the feasibility of measuring temperature maps using the PRF shift method. The accuracy of the PRF shift method increased when the B_0 drift effects were quantified and dismissed, indicating a PRF reading accuracy differing less than 0.5 °C from the thermometer. Results also validate our heating and temperature imaging protocol. This study is a valuable contribution to the evaluation of heating effects caused by RF absorption and demonstrates potential impact on future thermal investigations, which may use different heating sources, as well validate thermal simulations.

Keywords: MR thermometry, 7T MRI, MRI safety, proton resonance frequency (PRF), temperature mapping.

***Corresponding author: Maíra M. Garcia,** Faculty of Electrical Engineering and Applied Natural Sciences, Westphalian University, Gelsenkirchen, Germany, and General and Theoretical Electrical Engineering (ATE), University of Duisburg-Essen, and CENIDE – Center of Nanointegration Duisburg-Essen, D-47048 Duisburg, Germany, e-mail: maira.b.garcia@studmail.w-hs.de.
Tiago R. Oliveira, Department of Biomedical Engineering, Federal University of ABC, São Bernardo do Campo, Brazil.
Khallil T. Chaim, Faculdade de Medicina FMUSP, Universidade de São Paulo, São Paulo, SP, Brazil
Maria C. G. Otaduy, LIM44, Hospital das Clinicas HCFMUSP, Faculdade de Medicina, Universidade de São Paulo, São Paulo, SP, Brazil.
Christian Bruns, Johannes Bernarding, Institute for Biometry and Medical Informatics, University of Magdeburg, Magdeburg, Germany.
Jan T. Svejda, Daniel Erni, General and Theoretical Electrical Engineering (ATE), University of Duisburg-Essen, and CENIDE – Center of Nanointegration Duisburg-Essen, D-47048 Duisburg, Germany.
Waldemar Zylka, Faculty of Electrical Engineering and Applied Natural Sciences, Westphalian University, Gelsenkirchen, Germany.

1 Introduction

During magnetic resonance imaging (MRI) procedures, the radiofrequency (RF) energy is used to promote spin excitation. Part of the absorbed energy is converted into tissue heating, which may pose a potential hazard for the patient, specifically at ultra-high fields. Patient safety is assessed through the SAR, defined as the power deposited in tissue per unit mass. In the human body, the RF deposition pattern depends on diverse aspects, such as dielectric tissue properties, anatomical geometry, pulse sequences, among others [1]. Numerical simulations usually obtain SAR predictions. An induced heating profile can be evaluated based on SAR values by solving the bioheat transfer equation. Heating and SAR correlation is non-linear and heterogeneous since the resulting temperature is a balance between local heat and cooling sources leveraged by thermal conduction, convection, and materials' thermal properties [1].

Temperature variations can be assessed experimentally using different MR thermometry techniques. Measuring temperature variations during an MRI procedure is essential for many safety reasons, such as evaluating the heating induced by RF energy absorption, for thermal therapies like high-intensity focused ultrasound ablation, and others. The proton resonance frequency (PRF) shift is one of the most widely used MR-based thermometry methods. The technique is based on the fact that the electron shielding of water varies linearly with the temperature. It allows spatio-temporal evaluations, is non-invasive, and relatively independent of tissue type

Open Access. © 2023 The Author(s), published by De Gruyter. This work is licensed under the Creative Commons Attribution 4.0 International License.

[2]. The method presents accurate results compared to results measured by temperature sensors during the MR procedure, mainly when necessary correction methods are applied [1, 2].

In this work, we created and characterized a homogeneous muscle-mimicking phantom to experimentally investigate the temperature rise caused by the RF absorption during 7T MRI. The RF transmission was done using a commercial birdcage head coil, and a temperature heating and imaging protocol was developed and applied. Four oil tubes were placed outside the phantom as reference to calibrate the B_0 drift effects. Temperature evaluation was done via digital thermometer and PRF shift method with and without B_0 drift correction. Results for the axial plane demonstrate the temperature increase via RF exposure and the improvement in measurement accuracy using the B_0 drift correction.

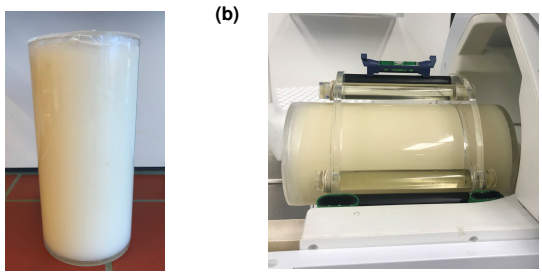

Fig. 1: (a) The homogeneous muscle-mimicking phantom. (b) Positioning of the phantom and oil tubes inside the coil. A non-magnetic spirit level was used to ensure horizontal alignment.

2 Materials and methods

2.1 Phantom preparation

The homogeneous muscle-mimicking phantom was manufactured following the recipes in [3] to simulate the dielectric, thermal, and MR properties of human tissues. It is a water-gelatine-oil-salt mixture, where the gelatine works as a gelling agent to avoid flow and thermal convection, NaCl controls the phantom's conductivity, and oil the permittivity. The phantom was created using 7.5594 g of NaCl, 200.6656 g of gelatine 240 bloom, 140.0 ml of canola oil, 12.6 ml of formaldehyde 37% (all from Carl Roth GmbH + Co, Germany), 1260.0 ml of deionized water and 8.0 ml of the surfactant Ecosurf^{TM} SA-9. The details of manufacturing are described in [3]. The mixture was inserted into a cylindrical support made of Plexiglas® (height = 200 mm, radius = 50 mm), as can be seen in Fig. 1(a).

The dielectric properties were measured using a dielectric assessment kit (DAK, Speag, Switzerland). Measurements were performed at 23 °C in 8 different regions of the phantom, repeated 10 times each. Phantom's conductivity and permittivity at 300 MHz were: $\sigma_p = 0.742 \pm 0.006$ S/m and $\epsilon_{r(p)} = 57.65 \pm 0.45$, respectively, which is in good agreement with the values obtained from the literature $\sigma_l = 0.771$ S/m and $\epsilon_{r(l)} = 58.2$ [4]. The measurements at the different regions showed very small variations of the dielectric properties.

2.2 RF heating and temperature imaging

The protocol to generate a temperature increase and at the same time monitor it was created, tested, and implemented at a 7T MRI scanner (MAGNETOM 7T, Siemens Healthcare, Germany) installed in São Paulo (Brazil) and Magdeburg (Germany). To heat the phantom, no external heating device was used. Solely T2-weighted turbo spin-echo (TSE) sequences were applied. The TSE is a standard clinical sequence that repeats in short time intervals the application of various refocusing RF pulses (180°), known to impose RF heating [5]. To monitor spatio-temporally the temperature increase, a multi-echo gradient-echo (GRE) sequence was applied.

The RF heating and temperature imaging protocol started with a pre-scan that includes: calibration, shimming, and B_1^+ field acquisitions. In sequence, GRE was applied to acquire the initial phase information for all three anatomical planes (axial, coronal, and sagittal) before heating. Next, the TSE sequence was applied twice, with no interval, 8.5 minutes in total. After that, GRE acquisitions were obtained for the three planes, followed by two TSE applications. The same steps were repeated until the end of the experiment ($t_{26} = 112$ min). Phase maps acquisitions were obtained at 27 time points: t_0, t_1, ..., t_{26}.

The TSE application was done to generate a large temperature increase. Its parameters were: echo-time $T_E = 24$ ms, repetition time $T_R = 5$ s, 180° flip angle, echo train length 20, 13 slices, 10 mm thickness. GRE parameters: $T_E = (2.5, 4, 5.5, 7)$ ms, $T_R = 10$ ms, 30° flip angle. For the axial plane 20 slices were acquired with 11.0 s of acquisition time, and for coronal and sagittal planes 13 slices were acquired with 7.3 s. Acquisitions were done for all phase-encoding directions and orientations, with 192 phase-encoding steps. In this work, just the results for the central axial plane measured with anterior-to-posterior (AP) phase-encoding direction and $T_E = 5.5$ ms are shown. In the PRF, using short GRE acquisitions guarantees a minimal heating/cooling of the phantom and therefore it can be considered that heating comes predominately from the TSE.

2.3 PRF shift temperature maps

For every time point t_f after the heating, i.e. $t_f > t_0$, the acquired GRE phase images were converted to maps of temperature differences $\Delta T_f = T_f - T_0$ using the PRF shift formula:

$$\Delta T_f = \frac{\phi_f - \phi_0}{\alpha\gamma B_0 T_E}, \quad (1)$$

where ϕ_0 is the phase information acquired at a time t_0, ϕ_f the phase information at time point t_f, γ the gyromagnetic ratio of hydrogen, B_0 the main magnetic field and α is the PRF coefficient (α = -0.01ppm/°C) [2]. To calculate the phase difference, the phase images were first rescaled and then unwrapped [6].

The accuracy of the PRF shift method can be substantially improved when doing corrections prospectively and/or retrospectively to the measurement. One correction method with a great impact on the results is the B_0 drift effect correction since the PRF shift method is very sensitive to phase changes. To quantify and correct the B_0 drift present during the experiment, four oil tubes were imaged along with the phantom. The phase changes that occur in oil are mostly caused by the B_0 drift, and less by the temperature [2]. The phase changes in each oil were measured and via interpolation of these values, phase correction maps over phantom's image region of interest (ROI) and over time were estimated. Each correction map is subtracted from the phantom's phase difference as:

$$\Delta T_f = \frac{(\phi_f - \phi_0) - (\phi_{oil_f} - \phi_{oil_0})}{\alpha\gamma B_0 T_E}. \quad (2)$$

The oil tubes (inner diameter = 12 mm, length = 130 mm) were placed outside and around the phantom using a structure made of Plexiglas®, as in Fig. 1(b). This setup was placed inside a commercial birdcage head coil for 7T (Nova Medical, USA). This is a coil with one channel of circular polarized transmission and a 32 channel receive array (1Tx/32Rx).

3 Results and discussion

To ensure initial thermal equilibrium, the phantom rested overnight in the MRI room. Phantom's initial and room temperature were T_0 = 17.4 °C. The phantom was quickly removed from the MRI room for the measurement of its isocenter temperature using a digital thermometer TP101 (Bmax, China). At the end of the experiment, the phantom's temperature was T_{26} = 20.5 °C. Using both initial and final temperature, a curve for $\ln(T/T_0)$ was generated and an interpolation was done to estimate the temperature values for each time moment in between (i.e. T_1 to T_{25}).

The relative temperature maps via PRF shift method were generated for all the anatomical planes and for each time intervals using (1). To improve the accuracy, the B_0 drift correction was implemented.

For the axial plane, eight phase differences were calculated subtracting the reference phase (ϕ_0) from each phase acquired after heating (ϕ_3, ϕ_6, ϕ_9, ϕ_{12}, ϕ_{15}, ϕ_{18}, ϕ_{21}, ϕ_{24}). In Fig. 2(a), the phantom's temperature change for different time intervals using PRF with and without B_0 drift corrections is shown. Temperature distribution in a horizontal line (red line in Fig. 2(a) at ΔT_{24}) for different time variations is shown in Fig. 2(b). The curves in Fig. 2(b) were plotted from raw data.

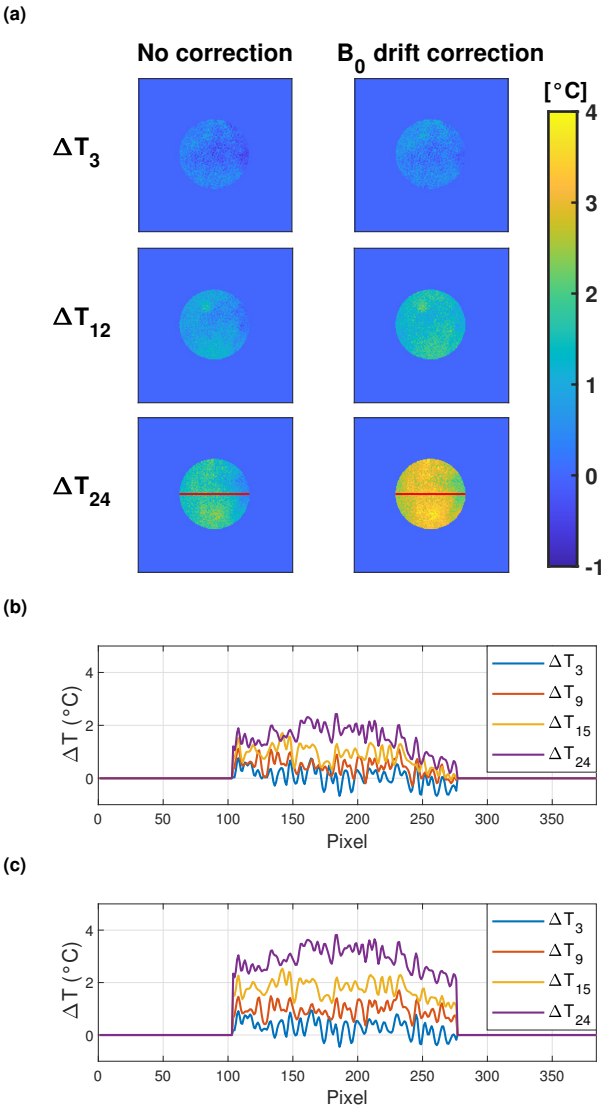

Fig. 2: (a) Phantom's temperature variation obtained via PRF shift technique with and without B_0 drift correction for the central axial slice. (b) The temperature variation along the central horizontal line in axial view from PRF without and in (c) with B_0 correction.

To estimate the temperature values via PRF shift, a calibration was done assuming the initial temperature from the thermometer as the same initial temperature for the central axial region (measured for a ROI with 3 pixels-radius around the central pixel). The central pixel temperature variations during the time can be seen in Fig. 3, where they were compared with the interpolated results obtained for the thermometer.

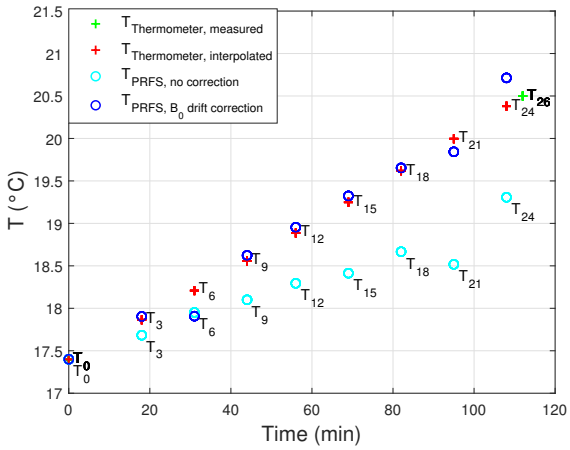

Fig. 3: Phantom's temperature for each specific time when an axial plane phase information was acquired. The temperatures T_0 and T_{26} measured with the digital thermometer and the interpolated values in between, as well the temperature values from PRF shift method without and with B_0 drift correction are presented.

As seen in Fig. 3, the curve for the PRF shift method without correction differs from the interpolated thermometer values, and its difference increases over time. The values obtained with the B_0 drift correction differ much less from the thermometer results. This demonstrates the improvement in the accuracy of the PRF shift method using oil for B_0 drift corrections, which is in accordance with the literature [1, 2]. The improvement in the accuracy can be seen in Table 1 for four different times. Observable is also the increase of the B_0 drift in time, effect that is well described in the literature. It is more noticeable in long MRI acquisitions and should be always taken into account for MR thermometry.

Results from Figs. 2 and 3 and Table 1 confirm that PRF shift method can provide time and spatial information from the RF absorption during 7T MRI. The PRF shift results observed after the B_0 correction show more accurate results when compared to the thermometer values. However, this study has some limitations. The temperature control can be done continuously using suitable probes, as fiber optic sensors, the heating protocol can be faster, as choosing less slices, planes or phase-encoding directions to analyze, among others. Such improvements will be applied to our next measurements.

Tab. 1: Central phantom's temperature acquired via digital thermometer and PRF shift with and without B_0 drift correction.

Temperature (℃)	T_3	T_9	T_{15}	T_{24}
PRF, no correction	17.68	18.10	18.41	19.31
PRF, B_0 drift correction	17.90	18.62	19.32	20.71
Thermometer, interpolation	17.86	18.56	19.25	20.38

4 Conclusions

This work analyzed the temperature rise in a muscle-mimicking phantom, which was exposed to RF heating applied by a birdcage head coil for 7T. The created phantom presented dielectric characteristics comparable with muscle tissue and its temperature was measured using a digital thermometer. Temperature variation measured via PRF shift presented an accuracy increase after correcting the B_0 drift effects using oil tubes. Results showed that the RF heating protocol elevated the phantom's temperature by around 3 °C, measured with both the thermometer and the PRF with B_0 drift correction. In this work, just the axial results were presented, but the same protocol was applied for coronal and sagittal planes, and the preliminary results are comparable. The thermal measurements present some limitations, which will be improved, such as using fiber optics sensors and making the GRE acquisition time faster by reducing the number of planes, slices, and/or phase-encoding directions.

Acknowledgment: We thank Gustavo D. Maia, Lucas M. Martins and Ewald Bonberg for technical assistance.

Author Statement: MMG was supported by the Brazilian agency CAPES: process n. 88881.173609/2018-01, and by the Westphalian University. Authors state no conflict of interest.

References

[1] Winter L, Oezerdem C, Hoffmann W, van de Lindt T, Periquito J, Ji Y, et al. Thermal magnetic resonance: physics considerations and electromagnetic field simulations up to 23.5 Tesla (1GHz). Radiat Oncol 2015;10:201.

[2] Hernandez D, Kim KS, Michel E, Lee SY. Correction of B_0 drift effects in magnetic resonance thermometry using magnetic field monitoring technique. Concepts Magn Reson 2016;46B:81-89.

[3] Yuan Y, Wyatt C, Maccarini P, Stauffer P, Craciunescu O, Macfall J, et al. A heterogeneous human tissue mimicking phantom for RF heating and MRI thermal monitoring verification. Phys Med Biol 2012;57(7):2021-37.

[4] Hasgall PA, Di Gennaro F, Baumgartner C, Neufeld E, Lloyd B, Gosselin MC, et al. IT'IS Database for thermal and electromagnetic parameters of biological tissues. 2022;4.1.

[5] Arduino A, Zanovello U, Hand J, Zilberti L, Brühl R, Chiampi M, et al. Heating of hip joint implants in MRI: The combined effect of RF and switched-gradient fields. Magn Reson Med 2021;85(6):3447-62.

[6] Herráez MA, Burton DR, Lalor MJ, Gdeisat MA. Fast two-dimensional phase-unwrapping algorithm based on sorting by reliability following a noncontinuous path. Appl Opt 2002;41(35):7437-44.